

# Identical-Location Transmission Electron Microscopy Study of Pt/C and Pt–Co/C Nanostructured Electrocatalyst Aging: Effects of Morphological and Compositional Changes on the Oxygen Reduction Reaction Activity

Flávio R. Nikkuni · Edson A. Ticianelli ·  
Laetitia Dubau · Marian Chatenet

Published online: 1 March 2013  
© Springer Science+Business Media New York 2013

**Abstract** In this study, the activity for the oxygen reduction reaction (ORR) and the structural, morphological, and compositional changes of Pt, Pt<sub>3</sub>Co, and PtCo nanoparticles deposited on high surface area carbon (Vulcan XC72) are investigated after they were submitted to accelerated electrochemical aging tests. These tests consisted of stepping the potential in 1 min successively between potentials of 0.9 and 0.1 V vs. reversible hydrogen electrode (RHE) or between 0.9 and 0.6 V vs. RHE for 15 h in 1.0 M H<sub>2</sub>SO<sub>4</sub> at 60 °C. Transmission electron microscopy, identical-location transmission electron microscopy, X-ray energy-dispersive spectroscopy analyses, and in situ X-ray absorption spectroscopy are used to characterize the changes in the morphological, compositional, and in the Pt 5d electronic states before and after the electrochemical aging tests. The experimental results show that the Pt/C and Pt–Co/C electrocatalysts are modified upon aging, following changes in particle size, geometry, and composition. The 0.9- to 0.6-V protocol is more aggressive in reducing the ORR activity, and this seems to be strongly related to the carbon corrosion and not to changes in the metallic particles. After the

0.9- to 0.1-V aging procedure, the ORR activity of the Pt/C particles is improved, while that of Pt<sub>3</sub>Co/C particles only slightly changes. In the case of Pt/C, these effects are related to the increase of the particle sizes, surface reconstruction, and, therefore, smaller oxide formation, which potentially induces an increase of the ORR activity. On the contrary, on Pt<sub>3</sub>Co/C, these positive effects are counterbalanced by a detrimental (and large) effect of Co dissolution.

**Keywords** Electrocatalyst degradation · ILTEM · Oxygen reduction reaction · Platinum and platinum–cobalt alloy nanoparticles

## Introduction

In the last few decades, the demand for clean and renewable energy has increased thanks to technological improvements and the massive (now worldwide) use of cell phones, portable computers, and other portable electronic devices. Moreover, the increasing concern about the use of fossil fuels renewed the interest for electric power system-motorized vehicles. For these portable/mobile applications, a promising electrical energy source is the proton exchange membranes fuel cell (PEMFC), which converts chemical energy directly into electrical energy. This is an auspicious energy source because it presents several good characteristics, including a relatively low operation temperature, cold start-up, high power density, high efficiency, and low pollutant emission [1]. However, PEMFCs still present a high cost due to the noble metal present in their electrodes and the use of the Nafion® membrane. An additional but nonetheless important technical problem is the slow kinetics of the oxygen reduction reaction (ORR). Large amounts of

**Electronic supplementary material** The online version of this article (doi:10.1007/s12678-013-0126-5) contains supplementary material, which is available to authorized users.

F. R. Nikkuni · E. A. Ticianelli (✉)  
Instituto de Química de São Carlos, Universidade de São Paulo,  
Avenida Trabalhador São-carlense, 400 Parque  
Arnold Schmidt, Caixa Postal 780,  
13560-970, São Carlos, São Paulo, Brazil  
e-mail: edsont@iqsc.usp.br

F. R. Nikkuni · L. Dubau · M. Chatenet  
Laboratoire d'Electrochimie et de Physico-chimie des Matériaux et  
des Interfaces LEPMI-Phelma, UMR 5279 CNRS/Grenoble-INP/  
Université de Savoie/Université Joseph Fourier, BP 75, 38402,  
Saint Martin d'Hères Cedex, France

studies are nowadays being conducted, aiming at cost reduction and improvement of ORR kinetics; in that extent, the electrocatalyst activity of Pt-based alloys dispersed on carbon, for example, PtV/C, PtFe/C, PtCo/C, PtNi/C, PtCr/C, is widely investigated [2–11].

Whatever their initial activity, it is important to state that such materials, and in particular the widely used Pt/C and PtCo/C electrocatalysts, do not present complete stability upon use in PEMFC [12–23]. In fact, in some of these works [20–23], the intentional leaching of Co on the particle surfaces of PtCo/C materials is explored for the formation of core–shell structures, leading to high active fuel cell catalysts. Although studying such electrocatalyst degradation after use in real PEMFC systems is mandatory [15–18], understanding the mechanisms of degradation may require additional experimentations, notably to directly follow what happens to the same group of metal/alloy nanoparticles upon aging. This is precisely the concept of identical-location transmission electron microscopy (ILTEM) [24] studies; these correspond to TEM analyses of the same physical object, before and after an electrochemical process. Up to now, only a few works use this technique for studies of the stability of dispersed Pt-based electrocatalysts regarding the features of the carbon support and of the metallic particles [25, 26] or studies of the degradation of Pt/C electrocatalysts at a high temperature in oxygen reduction reaction conditions [27, 28]. In these works, the electrocatalyst degradations were assigned mostly to carbon corrosion and particle agglomeration, growth, detachment from carbon, and dissolution/re-deposition processes. More recently, Yu et al. [29] presented images of electron tomography and electron energy loss spectroscopy imaging before and after voltammetric cycling of Pt<sub>3</sub>Co/C electrode between 0.6 and 1.0 V vs. reversible hydrogen electrode (RHE) and between 0.05 and 1.2 V vs. RHE (30,000 times,  $\nu=50$  mV s<sup>-1</sup>). The prominent effects were particle growth by coalescence, some particle movement over the carbon support, and also formation of some thin Pt shells. Schlögl et al. [26] and Meier et al. [30] showed results of identical-location scanning transmission electron microscopy and identical-location scanning electron microscopy to characterize the changes of a Pt<sub>3</sub>Co/C nanocatalyst after the degradation by potential cycling in 0.1 M HClO<sub>4</sub> between 0.4 and 1.4 V vs. RHE up to 7,200 times at 1.0 V s<sup>-1</sup>. Particle agglomeration, growth, dissolution and coalescence, and carbon corrosion were the more important phenomena occurring during the accelerated aging test.

In this work, the evolution of the structural and morphological markers and of compositional changes in Pt/C, PtCo/C, and Pt<sub>3</sub>Co/C electrocatalysts were investigated after they were submitted to accelerated electrochemical aging tests, conducted by successive potential stepping between 0.1 and 0.9 V vs. RHE and between 0.6 and 0.9 V vs. RHE in 15 h at a temperature of 60 °C and in 1.0 M H<sub>2</sub>SO<sub>4</sub> solutions. A special feature of the TEM analyses was the observation of the same physical object

before and after the aging process using the ILTEM technique [24]. Finally, X-ray absorption spectroscopy (XAS) was used to characterize the changes in the Pt 5d electronic states before and after electrode cycling. The overall goal of the work was to establish correlations between the electrochemical activity of the electrocatalysts for the oxygen reduction reaction and the changes occurring in the morphology and composition after aging processes.

## Experimental

The electrochemical experiments were conducted in a conventional three-electrode cell using a rotating disk electrode with active layers formed by commercial E-Tek catalysts Pt/C (lot A0820623), Pt<sub>3</sub>Co/C (lot A1240916), or PtCo/C (lot not available), deposited on a glassy carbon disk (diameter, 5 mm). The active layer precursor was a suspension formed by 2 mg of the nanocatalyst powder, 2 mL of isopropanol and 25  $\mu$ L of a 5 % Nafion<sup>®</sup> solution. After homogenization in an ultrasonic bath, an aliquot was deposited over the disk in order to have a charge of 20  $\mu$ g cm<sup>-2</sup> of metal. After drying, a film of Nafion<sup>®</sup> was formed to ensure that the electrocatalyst particles would not drop out from the glassy carbon disk surface (or the TEM grid; see below). The secondary electrode was a Pt foil and the reference was the saturated calomel electrode in the same electrolyte of the cell. All potentials are, however, expressed on the RHE scale in this study. All solutions were prepared with ultrapure water from a Milli-Q system and ultrapure sulfuric acid (99.9 %, J.T. Baker).

The working layer was firstly investigated for the evaluation of the specific area by the CO-stripping method and then for the ORR. Then, the particles were aged to evaluate the stability of the Pt/C and Pt<sub>x</sub>Co/C alloy nanoparticles, followed by another evaluation of the specific area (to quantify the ECSA losses) and of the ORR activity. For aging the nanoparticles, two steps of potential were alternately applied to the electrode at every 60 s, up to a total aging time of 15 h. The temperature was kept at 60 °C and the electrolyte was H<sub>2</sub>SO<sub>4</sub> 1.0 mol L<sup>-1</sup>. The potential steps used were 0.9–0.6 V vs. RHE and 0.9–0.1 V vs. RHE. Simultaneous measurements of the variation of the work and the counter electrode potentials during these aging cycles evidenced that the counter electrode potentials remains in the Pt oxide region, where the Faradaic reaction is mainly related to the oxygen evolution, since surface Pt oxides protect the underlying platinum atoms from dissolution, the effect being superior for bulk than for nanoparticle platinum surfaces [31, 32]. Also, the potential distribution along the working electrode surface is supposed to be very uniform because the currents were always very small (smaller than 1 mA in the ORR experiments), and so the ohmic drop was negligible.

The electroactivity for the oxygen reduction reaction was evaluated in  $1.0 \text{ molL}^{-1} \text{ H}_2\text{SO}_4$  electrolyte saturated with oxygen (Air Liquide, high purity), with the working electrode rotating from 400 to 2,500 rpm (Tacussel rotating disk electrode) and the potential cycled between 1.05 and 0.3 V vs. RHE. The CO-stripping method consisted of saturating the electrolyte with CO (Air Liquide, high purity) at low potential at enough time to form a CO monolayer over the electrocatalyst surface (approx. 6 min.); then, the dissolved CO was purged with inert gas and the voltammogram was recorded mainly to be used to calculate the specific Pt area.

For all TEM and ILTEM experiments, a JEOL 2010 TEM apparatus was used. This microscope is equipped with a LaB<sub>6</sub> filament operating at 200 kV (point-to-point resolution, 0.19 Å) and an X-ray energy dispersive spectrometer (X-EDS, Oxford, INCA®) probe. In the case of the ILTEM experiments, the same coating was used as for the aging experiments, and this was formed by a single drop added over a 300-mesh Au grid with Lacey carbon (EMS) specimen holder; the images were taken in the same region before and after electrocatalyst aging.

The electrocatalysts were also analyzed with in situ XAS, which was performed in the X-ray absorption near edge structure (XANES) region at the Pt L<sub>3</sub> absorption edge in the transmission mode. The spectroelectrochemical cell was projected to run in situ experiments with the membrane-electrode assembly at 25 or 80 °C. The working electrode was prepared by pressing the electrocatalyst agglutinated with a Nafion® membrane in a 0.7-cm<sup>2</sup> electrode area containing 6 mg Pt per square centimeter. The secondary (counter) electrode was an ordinary gas diffusion electrode containing Pt/C E-Tek as the electrocatalyst, with a hole which allows the X-ray beam to have a free pass. The measurements were carried out polarizing the electrode at 0.5 V vs. RHE and 0.9 V vs. RHE; the cell temperature was set 25 and 80 °C for each polarizing potential. All XAS measurements were carried out at the LNLS (Brazilian Synchrotron Light Laboratory) at the XAS beam line, in which the data acquisition system consists of three ionizing chambers (incidence  $I_0$ , transmitted  $I_t$ , and reference  $I_r$ ) acting as detectors; the reference chamber is mainly used for internal calibration of the edge position using a Pt foil. The computer program used for the analysis of the XAS data was the WinXAS package. Data analysis was done according to procedures described in the literature [33].

## Results

### Effects of the Electrode Potential Cycling on the Composition and Structure of the Electrocatalyst

Figure 1 shows the cyclic voltammograms obtained at  $20 \text{ mVs}^{-1}$  in  $1.0 \text{ molL}^{-1} \text{ H}_2\text{SO}_4$  for the as-received Pt/C and Pt<sub>3</sub>Co/C

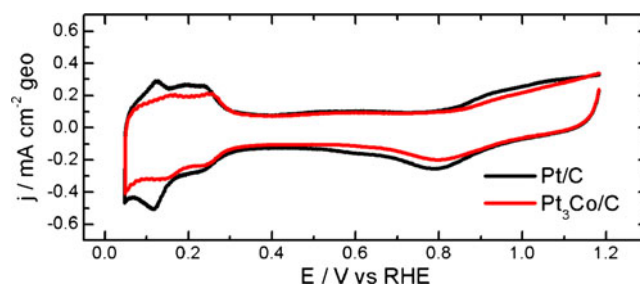


**Fig. 1** Cyclic voltammograms of Pt/C and Pt<sub>3</sub>Co/C plotted at  $\nu = 20 \text{ mVs}^{-1}$  in  $1.0 \text{ molL}^{-1} \text{ H}_2\text{SO}_4$

electrocatalysts. Both voltammograms are similar, although the currents related to the hydrogen adsorption/desorption and oxide/hydroxide formation at platinum sites are smaller for Pt<sub>3</sub>Co/C, as expected due to the smaller Pt content and electronic/strain effects induced by Co [15]. To evaluate the electrochemically active Pt surface area of the electrocatalysts, CO-stripping experiments were made for all electrocatalysts before and after the two aging protocols (the results are shown in Figs. 2 and 3 for the 0.9–0.1 V vs. RHE and 0.9–0.6 V vs. RHE aging tests, respectively). The values of the surface area (included in the corresponding figures) were obtained assuming that the oxidation of a full monolayer of adsorbed CO involves  $420 \mu\text{Ccm}^{-2}$ .

The results before and after the 0.9–0.1 V vs. RHE aging test (Fig. 2a) indicate similar behaviors for the Pt/C and Pt<sub>3</sub>Co/C electrocatalysts: a negative shift of the CO-stripping peak potential and a little loss of active area is monitored. The shift of the CO oxidation peak may be a consequence of a negative shift of the potential of Pt oxide formation, indirectly signing an increase of mean particle size upon aging [34]. The loss of peak area follows the decrease of the electrochemically active area of the samples due to either an increase of the mean particle size (in agreement with the negative shift of the peak) or some extent of electrocatalyst dissolution. The latter is, however, not as probable as for the 0.9–0.6 V vs. RHE aging protocol (Fig. 2b): the corresponding CO-stripping voltammograms show that only Pt/C presents a significant positive shift in peak potential after the aging, accompanied by a decrease of the active area. In this case, the potential alternates in a more anodic potential range, so the re-deposition of the Pt<sup>2+</sup> formed at the high potential is not likely at 0.6 V vs. RHE, in contrast to the lower vertex potential of 0.1 V vs. RHE. This means that the overall amount of Pt may essentially decrease by simple dissolution, yielding an overall decrease of the mean particle diameter. The behavior of PtCo/C slightly differs from those of Pt/C and Pt<sub>3</sub>Co/C: a non-negligible decrease of the active area is monitored, but with minimal changes of shape/potential of the CO-stripping peak.

**Fig. 2** Cyclic voltammograms of a CO monolayer oxidation (CO stripping) for Pt/C, Pt<sub>3</sub>Co/C, and PtCo/C before and after aging at 20 mVs<sup>-1</sup> in 1 molL<sup>-1</sup> H<sub>2</sub>SO<sub>4</sub> for the 0.9–0.1 V vs. RHE aging (a) and for the 0.9–0.6 V vs. RHE aging (b) protocols

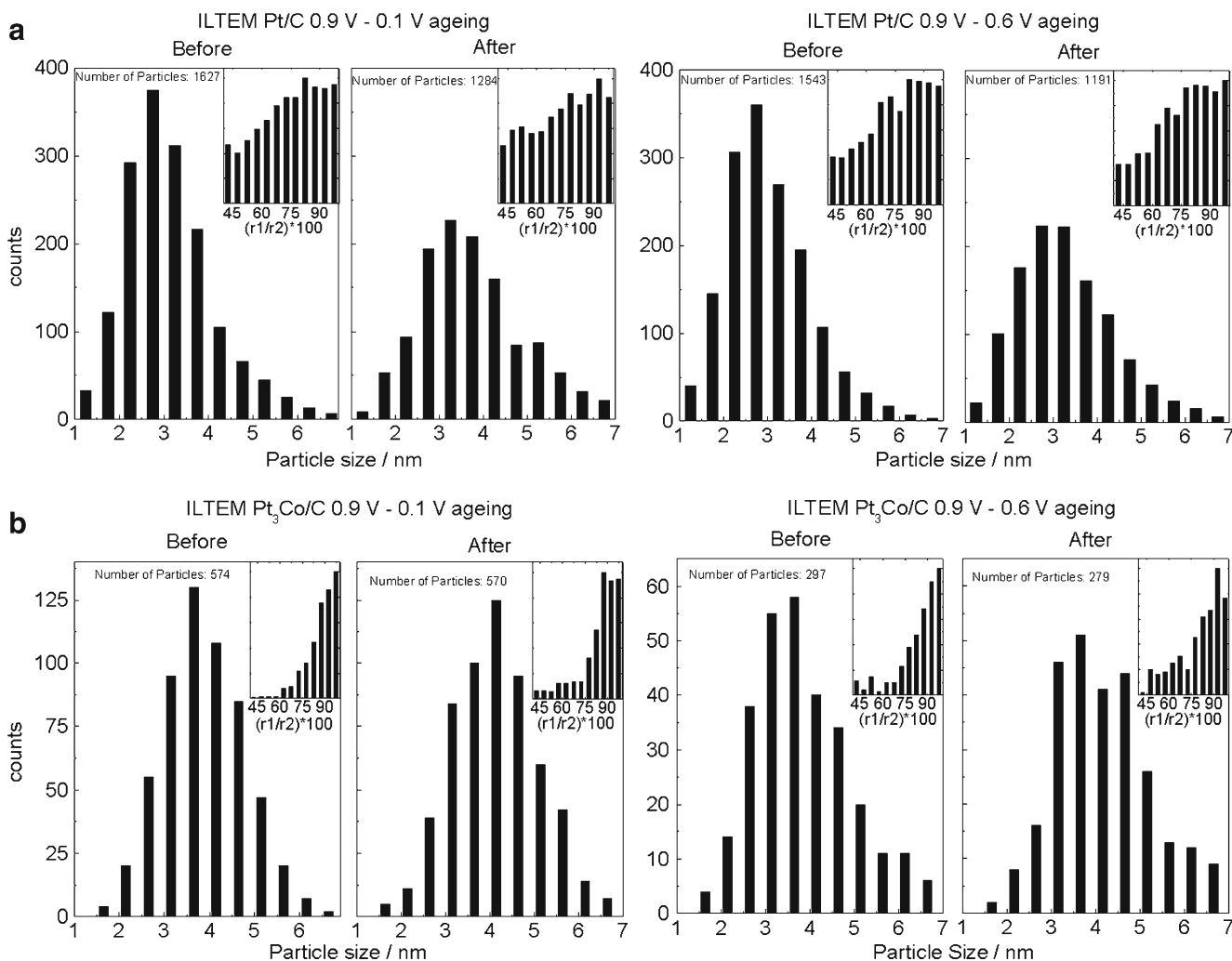
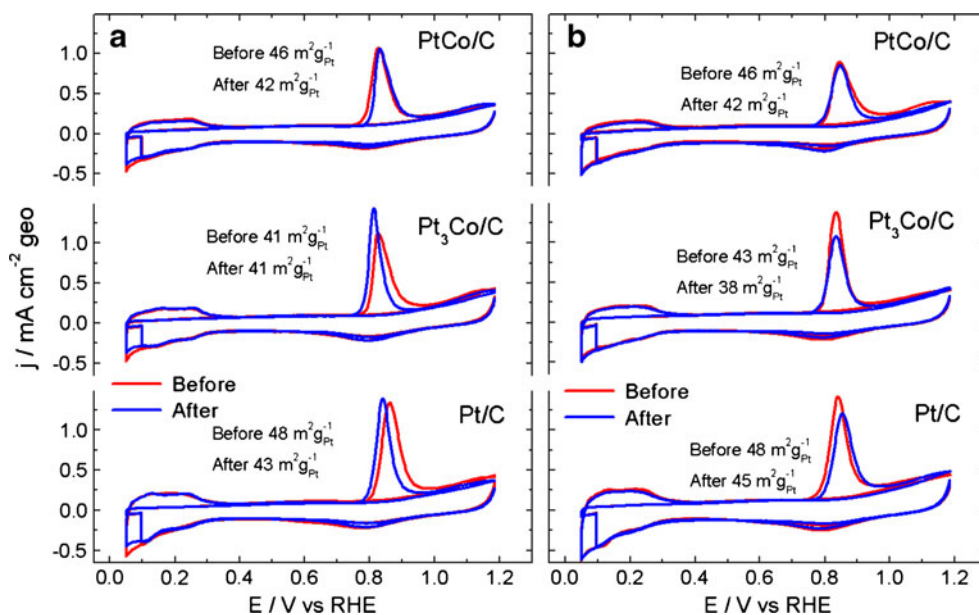


**Fig. 3** Histograms obtained from ILEM micrographs for Pt/C and Pt<sub>3</sub>Co/C before and after aging. *Insets* are the frequency for particle sphericity, obtained from  $r_1/r_2$ , where  $r_1$  is the larger diameter and  $r_2$  the smaller measured on the corresponding nanoparticle



**Table 1** Composition of the electrocatalysts before and after aging, as obtained by X-EDS analyses

Samples	Before				After			
	As-received		As-suspension		0.9–0.1 V vs. RHE		0.9–0.6 V vs. RHE	
	Pt (at%)	Co (at%)	Pt (at%)	Co (at%)	Pt (at%)	Co (at%)	Pt (at%)	Co (at%)
Pt <sub>3</sub> Co/C	74	26	73	27	87	13	86	14
PtCo/C	53	47	76	24	89	11	90	10

Table 1 presents the results of the X-EDS analyses of the PtCo<sub>x</sub>/C electrocatalysts before and after the aging processes. The column named “as-suspension” shows the results for the electrocatalyst deposited on the TEM grid from a suspension in isopropanol and Nafion® solution, the same used to prepare the active layer coating on the carbon disk electrode. The results for the as-received and as-suspension Pt<sub>3</sub>Co/C samples are very similar, indicating that the manipulation of the material during the preparation of the thin porous catalytic layer (TPC) does not change its characteristics. In the case of PtCo/C, the as-received sample presents the expected composition, while the as-suspension material presents a composition similar to that of Pt<sub>3</sub>Co/C. This demonstrates large Co leaching during the TPC preparation and the final composition of the material is very much similar to Pt<sub>3</sub>Co/C, which explains why the CO-stripping behavior of PtCo/C is less changed upon aging compared to Pt<sub>3</sub>Co/C (Fig. 2). Table 1, however, evidences a large dissolution of cobalt (starting from the as-suspension state) after the aging processes for both PtCo<sub>x</sub>/C electrocatalysts: whatever the initial composition, the final compositions stabilized at a Pt/Co proportion of 87–90:13–10 at%.

TEM images of the as-received and aged electrocatalysts are shown in Electronic supplementary material (ESM) Fig. S1. Before cycling, all electrocatalysts are very homogeneous in terms of particle sizes and distributions. Also, the aging tests (which both consist of rather mild aging conditions) did not dramatically change the particle morphology, but a more detailed discussion of this issue will be made below based on the ILTEM results. The histograms obtained for Pt/C, Pt<sub>3</sub>Co/C, and PtCo/C nanoparticles before and after the aging treatments are given in ESM Fig. S2; the PtCo/C histograms are similar to those for Pt<sub>3</sub>Co/C, which is not surprising owing to the fact that both materials exhibit rather similar morphology/compositions in their “as-suspension” state. Histograms denoted as “isolated” correspond to the counting of about 700 individual particles distributed along the TEM image, while the histograms labeled as “agglomerated” were obtained measuring and counting the mean diameter of groups of particles that could not be visualized separately from those in the neighborhood. These data are very valuable because, as described by Meier et al. [30] and Vion-Dury et al. [35], the agglomerated particles may play an important role in the process of degradation and the electroactivity of the

electrocatalyst by eventually coalescing or fusing with each other.

The histograms (ESM Fig. S2) evidence an increase of the mean particle size after the 0.9–0.1 V vs. RHE aging test for all catalysts. This was not the case for 0.9–0.6 V vs. RHE, which agrees with the electrochemical characterization results and signs that, whether Pt dissolution into Pt<sup>z+</sup> species can occur at the upper potential (0.9 V vs. RHE), Pt<sup>z+</sup> re-deposition on the remaining (larger) Pt crystallites is only likely at the lower potential limit of 0.1 V vs. RHE. In both cases, a broadening of the particle size distribution histogram is observed, meaning that the sizes of the particles are less homogeneous after than before. Also, these results clearly denote an increase of the number of agglomerates in the cycled samples, particularly for the 0.9–0.6 V vs. RHE protocol.

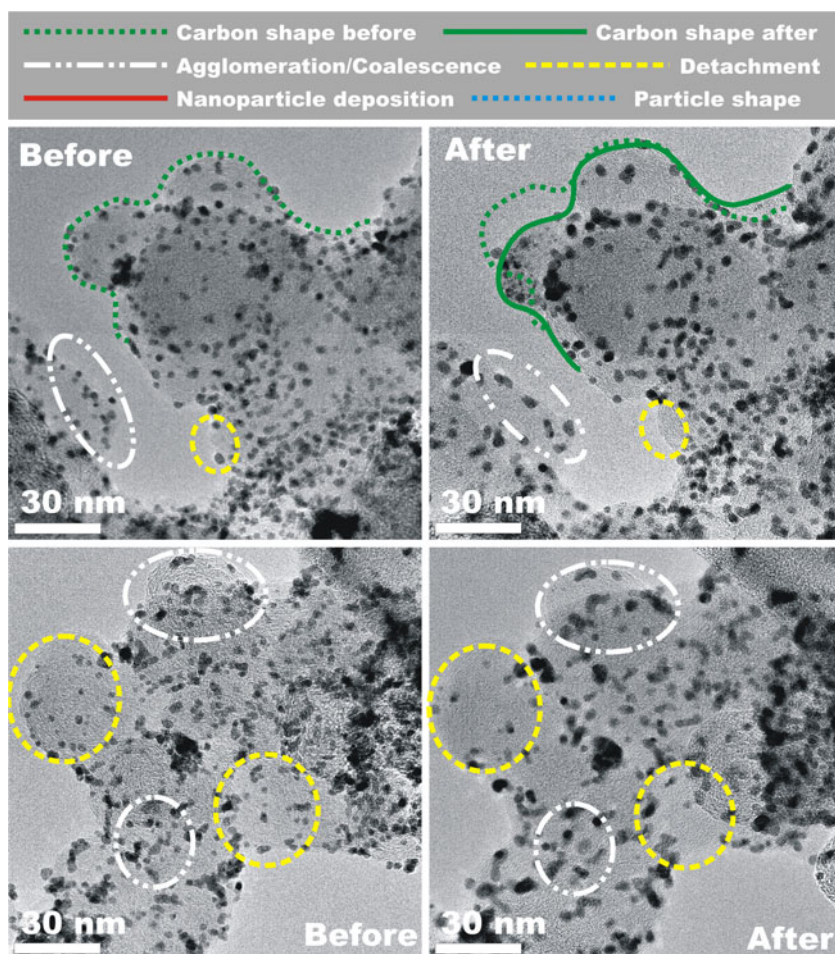
The ILTEM histograms obtained for Pt/C and Pt<sub>3</sub>Co/C before and after the aging treatments are given in Fig. 3. The corresponding mean particle sizes are summarized in Table 2. The estimated error for the particle size determinations on the TEM pictures, as described above, is about ±0.2 nm (1 pixel amount 0.15 nm in the images), but the particles were nevertheless ranged for diameter increments of 0.5 nm on the particle size distribution histograms. Whatever the electrocatalysts considered, the particle size distribution obtained basically confirms those obtained from conventional TEM.

The inserts in the histograms (ESM Figs. S2 and 3) show plots of the relative frequency as a function of the ratio between the largest ( $r_2$ ) and smallest diameters ( $r_1$ ) of a given particle in a way that when  $r_1=r_2$  the particle is

**Table 2** Mean particle sizes obtained before and after aging, as measured by TEM and ILTEM

Samples	Mean particle size			
	0.9–0.1 V vs. RHE		0.9–0.6 V vs. RHE	
	Before	After	Before	After
Pt/C	3.0	3.6	3.0	3.1
Pt <sub>3</sub> Co/C	3.6	4.4	3.6	3.7
PtCo/C	3.1	3.6	3.1	3.3
ILTEM Pt/C	3.2	3.9	3.0	3.3
ILTEM Pt <sub>3</sub> Co/C	4.0	4.3	4.0	4.4

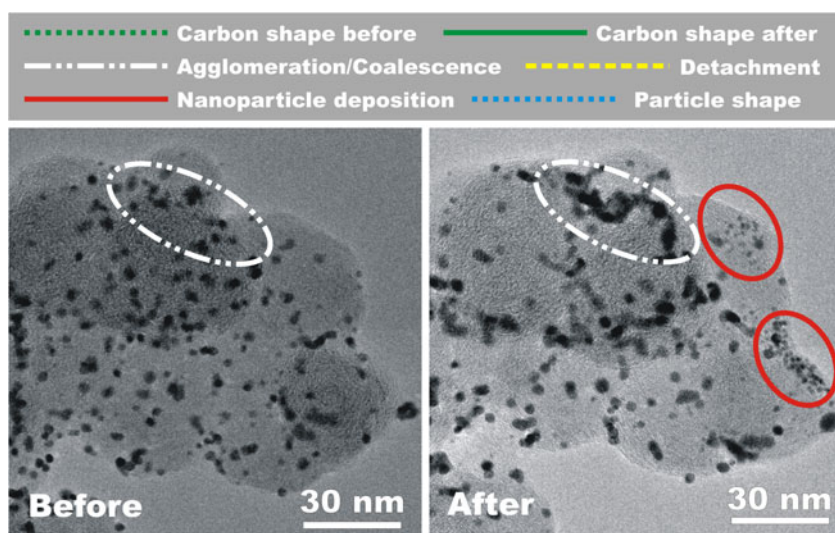
**Fig. 4** Micrographs obtained by ILTEM technique for the same regions of Pt/C before and after the 0.9–0.1 V vs. RHE aging test (regions 1 and 2)



approximately spherical, independently of its size. The distributions for Pt/C and Pt<sub>3</sub>Co/C are similar, showing that whatever the composition of the initial electrocatalyst the particles become little less spherical after the aging protocols. This phenomenon may be assigned to the agglomeration/coalescence of two or more particles, so that

the ratio of the new particles is increased compared to the former ones. Pt/C seems to have more irregular particles, with less “sphericity” than the Pt<sub>x</sub>Co/C electrocatalysts (in particular, this effect is not very pronounced for Pt<sub>3</sub>Co/C), indicating that the PtCo<sub>x</sub>/C materials are more stable against degradation by coalescence in these aging conditions.

**Fig. 5** Micrographs obtained by the ILTEM technique for the same regions of Pt/C before and after the 0.9–0.1 V vs. RHE aging test (region 3)





Figures 4, 5, 6, 7, 8, 9, and 10 represent the ILTEM micrographs obtained before and after the two aging procedures for Pt/C and Pt<sub>3</sub>Co/C. ILTEM histograms allow quantifying the changes of a number of particles for the considered carbon grains, which is useful for the quantitative analysis of the electrocatalyst degradation [35]. They can also demonstrate whether the electrochemical aging tests modify the Pt or Pt<sub>3</sub>Co particles (morphology and composition). The structural degradations observed from the results in Figs. 4, 5, 6, 7, 8, 9, and 10 are multifold: changing shape of carbon, following its corrosion (green lines), loss of particles (dashed yellow lines), and, eventually, agglomerating or coalescing (white dashed traced lines). This last effect is surely responsible for the increase of the mean particle size and a reduction of their sphericity, as noted in Fig. 3 and ESM S2.

In particular, the Pt/C electrocatalyst undergoes a considerable loss of particles (by approx. 21 and 23 % for the 0.9–0.1 V vs. RHE and 0.9–0.6 V vs. RHE aging tests, respectively), resulting in a lower particle density onto the carbon substrate (Figs. 4, 5, and 6). In the former case (0.9–0.1 V vs. RHE aging test), the particles are subjected to severe agglomeration/coalescence, with

concomitant loss of particle density at the carbon surface (Fig. 4) and an increase in average size (from 3.0 to 3.6 nm; Table 2), which makes their sphericity decreases understandable (Fig. 3). This likely follows into a large extent crystallite migration and Ostwald ripening, the latter being emphasized because Pt<sup>z+</sup> re-deposition is very likely at the lower potential limit of 0.1 V vs. RHE. In the latter case (0.9–0.6 V vs. RHE aging test), the pronounced loss of particles mainly stems from the irreversible dissolution of the particles (Pt<sup>z+</sup> re-deposition is not likely at the lower potential limit of 0.6 V vs. RHE) or their detachment from the carbon substrate following its corrosion. As a result, agglomerates are formed (Fig. 6), but the isolated particles do not grow drastically in size (slight increase from 3.0 to 3.1 nm; Table 2). From these differences, one understands the clear impact of the lower vertex potential: 0.1 V vs. RHE favors Pt<sup>z+</sup> re-deposition, but also the coalescence (recrystallization) of the particles, whereas at 0.6 V vs. RHE, the permanent carbon and Pt corrosion favors Pt particle agglomeration and irreversible dissolution (as also demonstrated in [28, 36]), respectively. In turn, particle sphericity is not severely affected by this aging procedure (Fig. 6).

**Fig. 6** Micrographs obtained by ILTEM technique for the same regions of Pt/C before and after the 0.9–0.6 V vs. RHE aging test

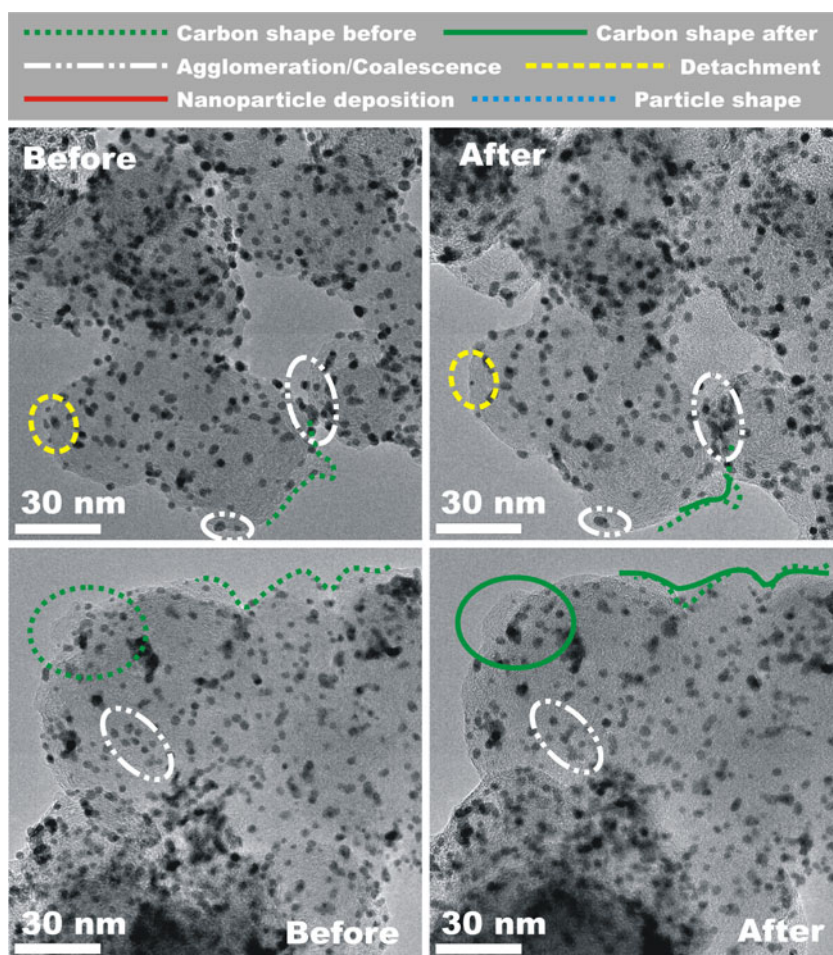
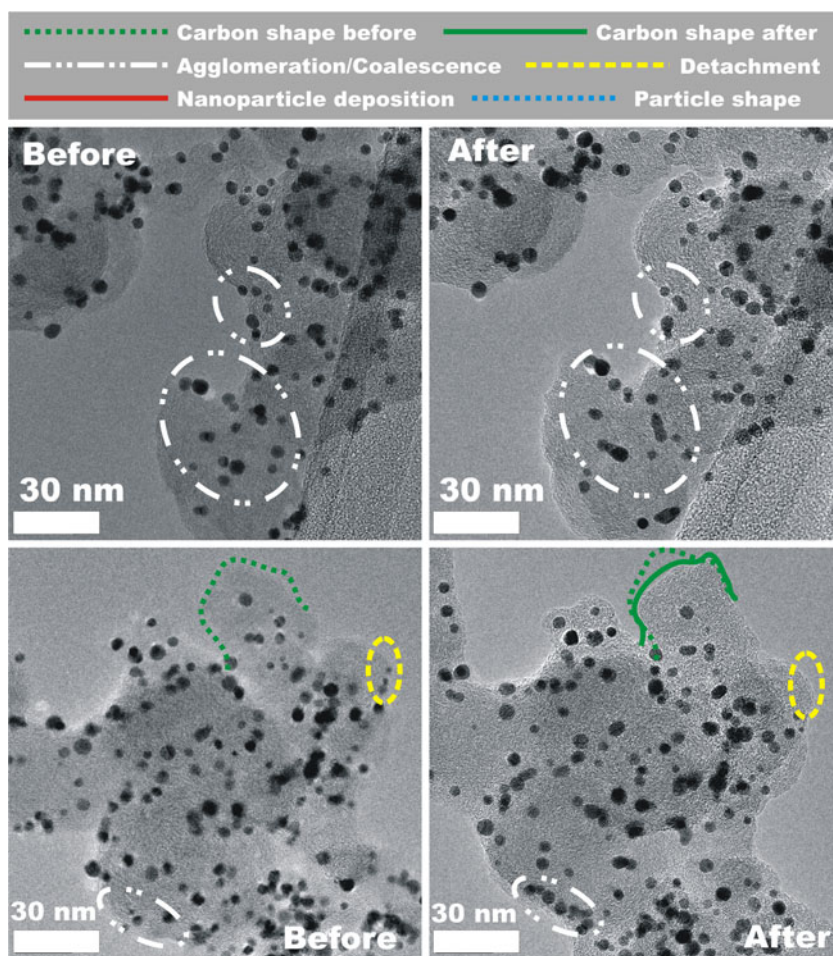


**Fig. 7** Micrographs obtained by ILTEM technique for the same regions of Pt<sub>3</sub>Co/C before and after the 0.9–0.1 V vs. RHE aging test



Regarding Pt<sub>3</sub>Co/C, one firstly notes that the number of particles on the carbon is nearly unchanged, only decreasing by a mere 6 % for 0.1 and 0.6 V vs. RHE as a lower vertex potential, respectively, (Fig. 3). Also, particle degradations seem overall less pronounced than for Pt/C, whatever the aging procedure (Figs. 7 and 8). From this prospect, it appears that Pt<sub>3</sub>Co/C is more stable than Pt/C in such accelerated aging tests. As the 0.9–0.1 V vs. RHE treatment especially favors carbon corrosion [35] (for Pt/C electrocatalysts), the present results for Pt<sub>3</sub>Co/C seem to show that the material is less subjected to such corrosion mechanism in these conditions; this can follow the role of “sacrificial anode” of Co [15, 17, 18, 37] or an indirect larger stability of the carbon substrate in contact with Pt<sub>3</sub>Co particles, which would be a “worse” carbon oxidation electrocatalyst than Pt particles. Concerning the 0.9–0.6 V vs. RHE aging test, the small decrease in the amount of particles may be assigned to a complete dissolution of the alloy or the particle loss due to carbon corrosion, but, once again, in a much less severe proportion than for Pt. For the particular case of Pt<sub>3</sub>Co/C upon the 0.9–0.6 V vs. RHE aging test, areas with metal re-deposition in very tiny particles were also found, probably embedded in Nafion® (red circle), contributing to a decrease of the specific activity for the ORR

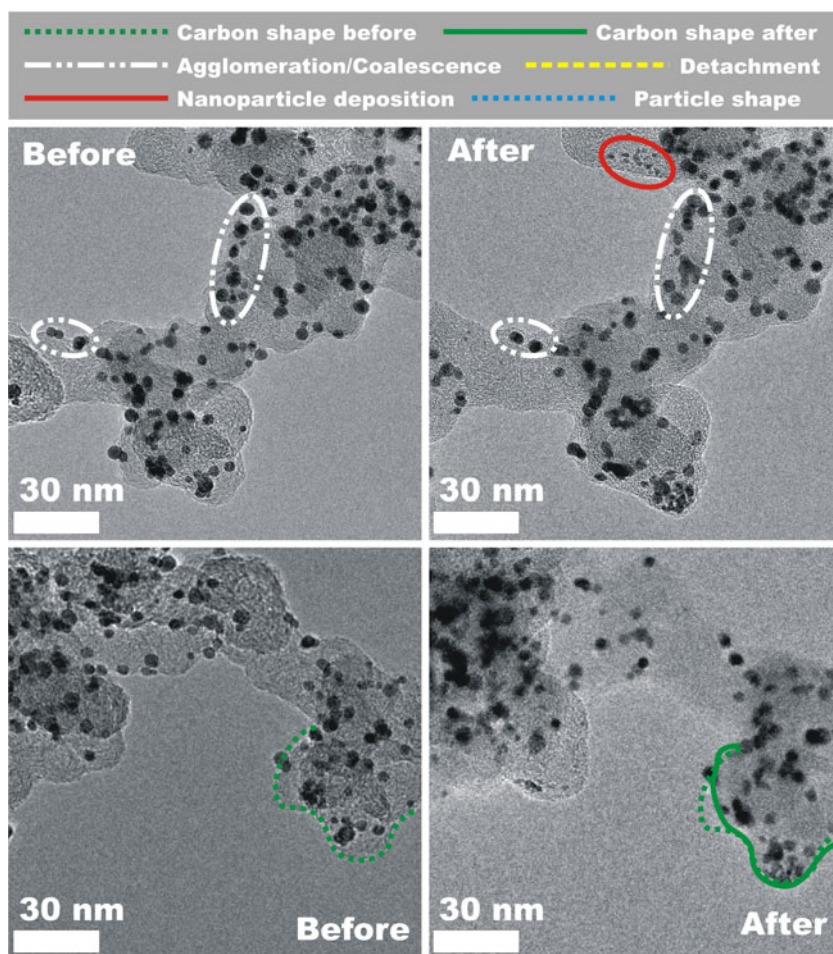
[38], and particles with a changed shape (blue dashed circle/hexagon), evidencing some faceting, which may also affect ORR specific activity (see “Activity for the ORR”).

#### XAS Characterization of the Pt/C and Pt<sub>3</sub>Co/C Electrocatalysts

Figures 10 and 11 show the XANES spectra (obtained at 80 °C and 0.5 V vs. RHE or 0.9 V vs. RHE, respectively) at the Pt L<sub>3</sub> edge that corresponds to 2p<sub>3/2</sub>–5d electronic transition. The magnitude of the hump (white line) located at approx. 11.572 eV (insert in the figures) reflects the occupancy of the 5d electronic state, following the Pauli principle [39]. The magnitude of the white line for Pt/C and Pt<sub>3</sub>Co/C at 0.5 V vs. RHE (Fig. 10a, b) is virtually the same, indicating that the Pt 5d band occupancy is essentially similar, thereby implying that the second metal has no large influence in the Pt electronic states at this potential, as expected because of the low Co content. The magnitude of the white line increases in both cases when measured at a higher potential, 0.9 V vs. RHE, showing that the Pt 5d band is more vacant at 0.9 V vs. RHE [9], but the effect is smaller for the Pt<sub>3</sub>Co/C electrocatalyst. This increase of the white line at 0.9 V vs. RHE is assigned to the oxidation of the Pt



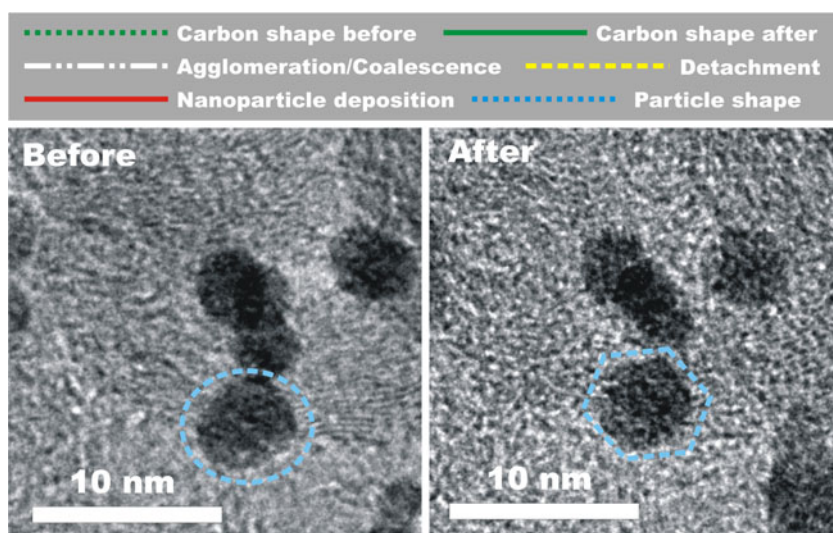
**Fig. 8** Micrographs obtained by ILTEM technique for the same regions of Pt<sub>3</sub>Co/C before and after the 0.9–0.6 V vs. RHE aging test



atoms in the particle surface, and so the smaller effect for Pt<sub>3</sub>Co/C may be a consequence of two factors: (1) a lower Pt content in the surface for the Pt<sub>3</sub>Co/C electrocatalyst particles and/or (2) a blocking of the Pt oxidation introduced by Co, as previously reported by Mukerjee et al. [39].

No differences are observed between the as-received electrocatalysts and the aged ones when the electrode is polarized at 0.5 V vs. RHE, confirming the small influence of the second metal on the properties of the Pt 5d electronic states at a low potential. This is not the case for 0.9 V vs.

**Fig. 9** Micrographs obtained by ILTEM technique for the same regions of Pt<sub>3</sub>Co/C before and after the 0.9–0.6 V vs. RHE aging test (increased resolution)



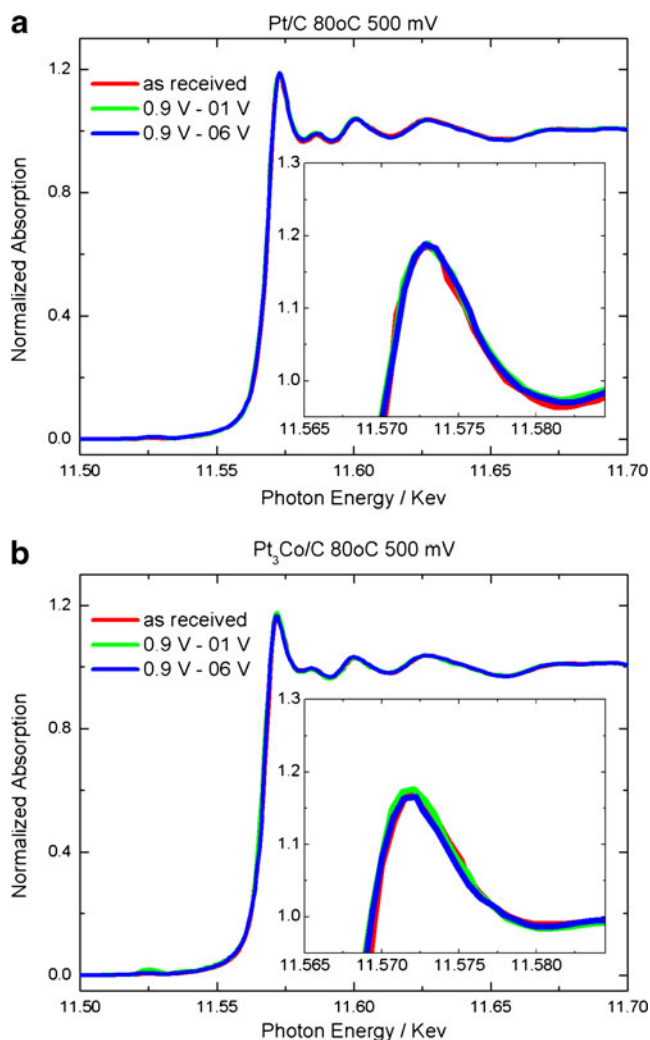


**Fig. 10** XANES spectra at the Pt  $L_3$  edge for the electrocatalysts at 0.5 V vs. RHE and 80 °C before and after aging protocols: Pt/C (a) and  $Pt_3Co/C$  (b)

RHE: in all cases, there was a lowering of the magnitude of the white line or a decrease of the Pt surface atom oxidation, which is, in any case, better for fast ORR (see “Activity for the ORR”); the largest effect is observed for the  $Pt_3Co/C$  electrocatalyst after the 0.9–0.1 V vs. RHE aging protocol.

For Pt/C, the effects observed on XAS experiments are mostly caused by the mean particle size (and, indirectly, the active surface area): the bigger the particle, the lower is the white line and the better is the ORR activity. As expected, the biggest area of the white line is measured for the “as-received” electrocatalyst, followed by those aged in the 0.9–0.6 V vs. RHE and the 0.9–0.1 V vs. RHE protocols; this will have non-negligible effects on the ORR activity (see “Activity for the ORR” and Table 3) [40].

As for Pt/C, the XAS experiments conducted for  $Pt_3Co/C$  at 0.9 V vs. RHE show lower formation of Pt oxides for the

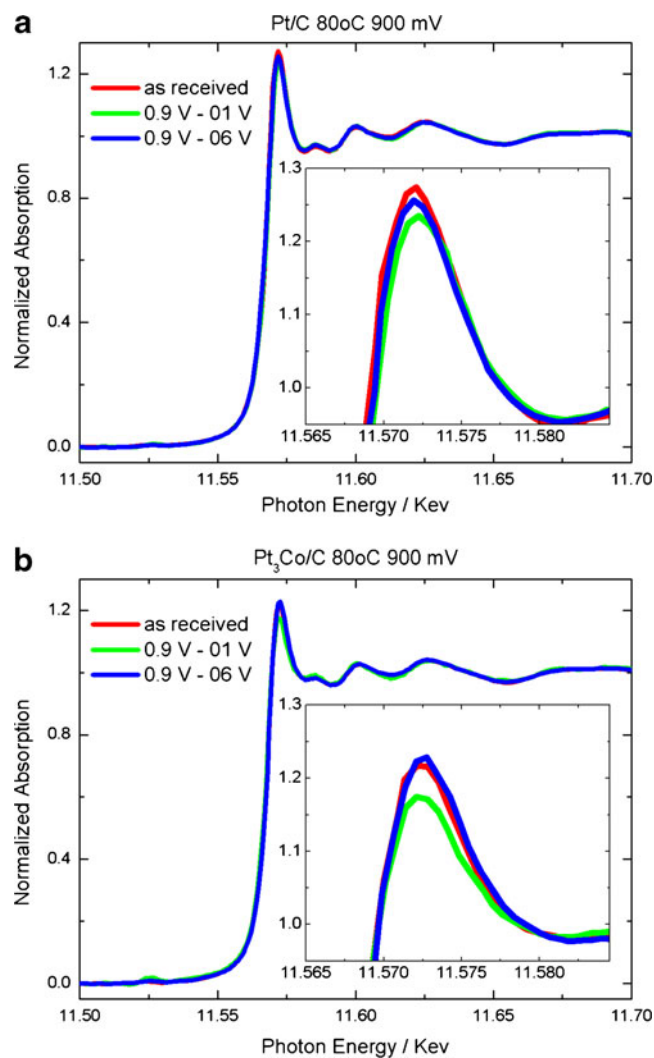


**Fig. 11** XANES spectra at the Pt  $L_3$  edge for the electrocatalysts at 0.9 V vs. RHE and 80 °C before and after aging protocols: Pt/C (a) and  $Pt_3Co/C$  (b)

0.9–0.1 V vs. RHE aging protocol; it is consistent with the lower potential limit of 0.1 V vs. RHE, which is compatible with Pt oxide ( $Pt^{z+}$ ) reduction and to the fact that bigger particles are observed for this sample, following Pt re-deposition upon corrosion at a high potential. However, this is not the electrocatalyst that is subjected to the largest active area losses (Fig. 2), once again because the electrochemical treatment favors  $Pt^{z+}$  re-deposition, indirectly leading to a particle surface with a low content of Co. This statement is confirmed by the voltammograms of Fig. 2, where, after the 0.9–0.1 V vs. RHE aging protocol, the hydrogen adsorption/desorption region is better defined, a sign of a Pt-like characteristic [15]. Concerning the results of the “as-received” and 0.9–0.6 V vs. RHE-aged electrocatalysts, the XAS results are coherent with the change of active area and those of ORR activity (see “Activity for the ORR”).

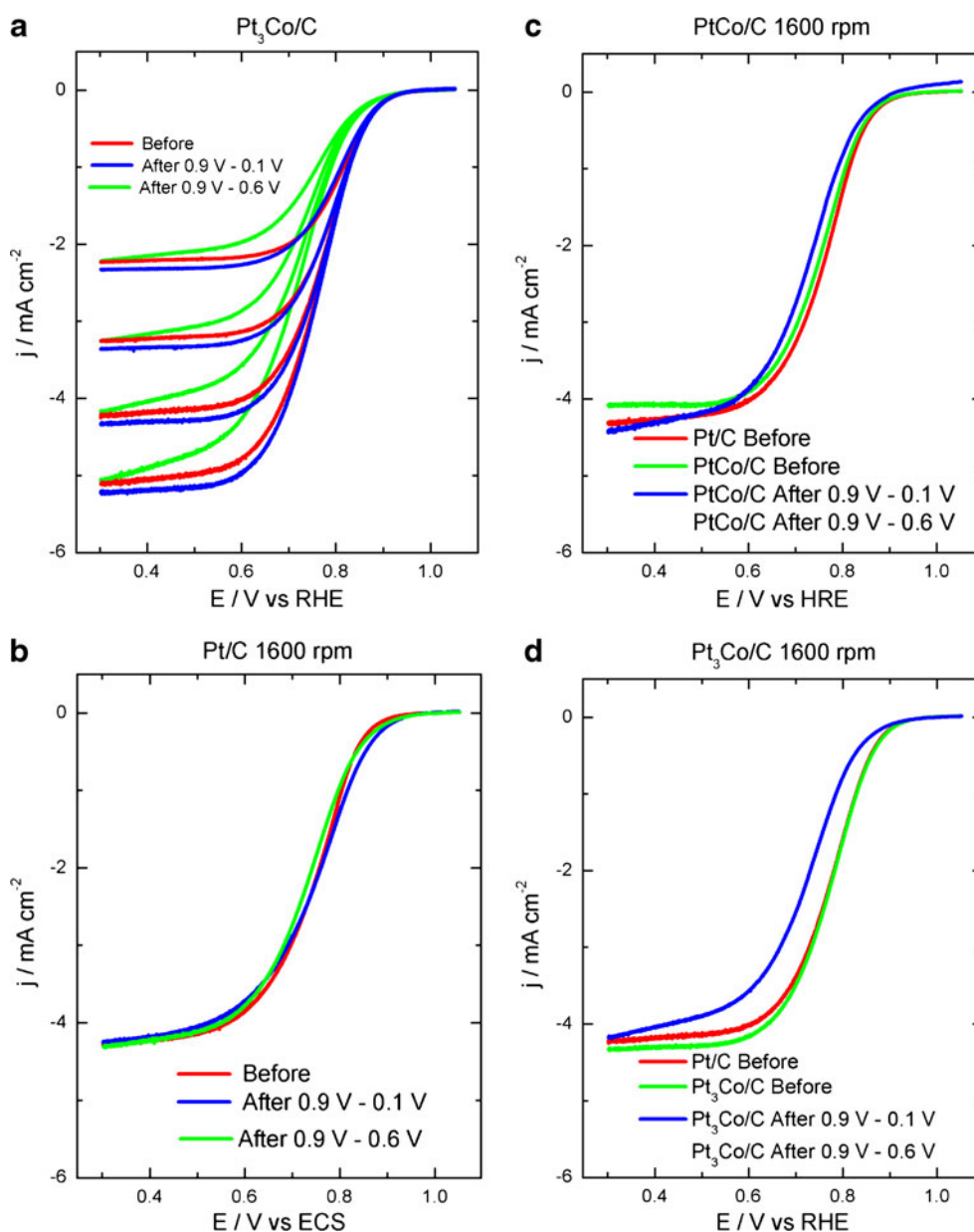
**Table 3** Specific activity before and after aging

Samples	Specific activity ( $\mu\text{A}/\text{cm}^2_{\text{Pt}}$ ) at 0.90 V				Specific activity ( $\mu\text{A}/\text{cm}^2_{\text{Pt}}$ ) at 0.85 V			
	0.9–0.1 V vs. RHE		0.9–0.6 V vs. RHE		0.9–0.1 V vs. RHE		0.9–0.6 V vs. RHE	
	Before	After	Before	After	Before	After	Before	After
Pt/C	6	14	8	14	27	48	34	43
Pt <sub>3</sub> Co/C	20	20	22	13	84	83	92	42
PtCo/C	14	14	16	10	60	56	73	41

## Activity for the ORR

Figure 12 presents the linear sweep voltammograms of oxygen reduction reaction plotted in quasi-stationary conditions at  $\nu=1 \text{ mVs}^{-1}$  and  $25 \text{ }^\circ\text{C}$  in  $1 \text{ molL}^{-1} \text{ H}_2\text{SO}_4$  before

and after the aging protocols. The polarization curves obtained as a function of the revolution rates present the typical activation/diffusion–convection-controlled profiles for this kind of electrodes either before or after the aging procedures. Table 3 summarizes the specific activity of the

**Fig. 12** Quasi stationary polarization curves for oxygen reduction reaction obtained in  $1.0 \text{ molL}^{-1} \text{ H}_2\text{SO}_4$  at  $\nu=1.0 \text{ mVs}^{-1}$ 



materials at 0.85 and 0.9 V vs. RHE (mass transport-corrected kinetic current measured at 0.85 and 0.9 V vs. RHE, respectively, divided by the surface area obtained by the CO-stripping experiments). Although in the case of the kinetic currents measured at 0.9 V there is dispersion (the values are reproducible within  $\pm 15\%$ , which is acceptable for kinetic parameters) due to the low magnitude of the experimental raw currents, the results at both potentials for Pt/C after the 0.9–0.1 V vs. RHE aging protocol clearly denote a small improvement in ORR specific activity (likely following the non-negligible average Pt/C particle size growth; Fig. 5 and Table 2), which can be explained by the well-known Pt particle size effect [41, 42] and the reduction of the surface coverage of Pt oxides (“XAS Characterization of the Pt/C and Pt<sub>3</sub>Co/C Electrocatalysts”). For both Pt–Co electrocatalysts, the activity remained essentially constant; although all the structural effects mentioned above are present after the 0.9–0.1 V vs. RHE aging test, in this case, the dissolution of the non-noble transition metal (Co) may introduce a negative effect (loss of geometric and/or strain effect induced by Co), and so the activity remains close to the one found in the beginning, as seen in Table 2 [15].

After the other protocol (0.9–0.6 V vs. RHE), the specific activity of Pt/C slightly increases (in agreement with the slight growth of the particle size; Fig. 5 and Table 2), while the Pt–Co/C electrocatalysts clearly exhibit reduced activity. Here, the effects of cobalt dissolution (the driving force for Co dissolution is larger at 0.6 V vs. RHE than at 0.1 V vs. RHE) and smaller re-deposition of Pt result in (1) depleted Co content (Table 1), (2) smaller (or at least not larger) nanoparticles (Table 2), and (3) large extent of Pt oxides at 0.9 V vs. RHE (Fig. 12), all effects being detrimental and yielding smaller activity for the ORR.

## Conclusions

In this study, the TEM and ILTEM characterizations of Pt/C and Pt–Co/C electrocatalysts clearly demonstrated that their structure and composition change after aging, mainly by changing the particle size and geometry and Co dissolution. The 0.9–0.6 V vs. RHE aging protocol is more aggressive in reducing the oxygen reduction reaction activity, and this seems to be strongly related to carbon corrosion and reduced average particle sizes. In opposition, the 0.9–0.1 V vs. RHE aging protocol yields smaller loss of ORR activity (or even increased activity for Pt/C), mainly because Pt<sup>z+</sup> re-deposition is likely at 0.1 V vs. RHE, thereby maintaining “larger” average particle size and, therefore, larger ORR activity. In the case of Pt/C, these effects are only related to the increase of the particle sizes, some surface reconstruction, and smaller oxide formation, which potentially induces an increase of the ORR activity. On the contrary, Pt<sub>3</sub>Co/C is subjected to large

Co dissolution, and this may (detrimentally) balance the above effects of the average particle size.

**Acknowledgments** The authors thank CNPq (project CTNERG: 577899/2008-2), Capes/Cofecub (project 598/08), FAPESP (project 09/07629-6), the Brazilian Nanotechnology National Laboratory (LNNano), the Brazilian Synchrotron Light Laboratory (LNLS), and Oseo-Anvar for financial supports (H2E project).

## References

1. W. Vielstich, A. Lamm, H. A. Gasteiger (2003) Handbook of fuel cells: fundamentals technology and applications, vol. 2. Electrocatalysis. Wiley, Chichester, pp. xi–xiv
2. L.G.R.A. Santos, K.S. Freitas, E.A. Ticianelli, *Electrochim. Acta* **54**, 5246 (2009)
3. A.C. Garcia, F.H.B. Lima, E.A. Ticianelli, M. Chatenet, *J. Power Sources* **222**, 305 (2013)
4. B. Narayanamoorthy, K.K.R. Datta, S. Balaji, *J. Colloid Interface Sci.* **387**, 213 (2012)
5. A.M.C. Luna, A. Bonesi, W.E. Triaca, A.D. Blasi, A. Stassi, V. Baglio, V. Antonucci, A.S. Aricò, *J. Nanoparticle Res.* **12**, 357 (2010)
6. W. Trongchuanvij, K. Pruksathorn, M. Hunsom, *Appl. Energy* **88**, 974 (2011)
7. F.H.B. Lima, W.H. Lizcano-Valbuena, E. Teixeira-Neto, F.C. Nart, E.R. Gonzalez, E.A. Ticianelli, *Electrochim. Acta* **52**, 385 (2006)
8. S. Koh, M.F. Toney, P. Strasser, *Electrochim. Acta* **52**, 2765 (2007)
9. A.C. Fernandes, V.A. Paganin, E.A. Ticianelli, *J. Electroanal. Chem.* **648**, 156 (2010)
10. L.G.R.A. Santos, C.H.F. Oliveira, I.R. Moraes, E.A. Ticianelli, *J. Electroanal. Chem.* **596**, 141 (2006)
11. M.K. Jeon, Y. Zhang, P.J. McGinn, *Electrochim. Acta* **55**, 5318 (2010)
12. P.J. Ferreira, G.J. Ia O, Y. Shao-Horn, D. Morgan, R. Makharia, S. Kocha, H.A. Gasteiger, *J. Electrochem. Soc.* **152**, A2256 (2005)
13. H.A. Gasteiger, S.S. Kocha, B. Sompalli, F.T. Wagner, *Appl. Catal. B Environ.* **56**, 9 (2005)
14. E. Guilminot, A. Corcella, F. Charlot, F. Maillard, M. Chatenet, *J. Electrochem. Soc.* **154**, B96 (2007)
15. L. Dubau, F. Maillard, M. Chatenet, J. André, E. Rossinot, *Electrochim. Acta* **56**, 776 (2010)
16. L. Dubau, F. Maillard, M. Chatenet, L. Guetaz, J. André, E. Rossinot, *J. Electrochem. Soc.* **157**, B1887 (2010)
17. F. Maillard, L. Dubau, J. Durst, M. Chatenet, J. André, E. Rossinot, *Electrochem. Commun.* **12**, 1161 (2010)
18. L. Dubau, J. Durst, F. Maillard, L. Guétaz, M. Chatenet, J. André, E. Rossinot, *Electrochim. Acta* **56**, 10658 (2011)
19. C.E. Carlton, S. Chen, P.J. Ferreira, L.F. Allard, Y. Shao-Horn, *J. Phys. Chem. Lett.* **3**, 161 (2012)
20. M. Oezaslan, M. Heggen, P. Strasser, *J. Am. Chem. Soc.* **134**, 514 (2012)
21. M. Oezaslan, F. Hasche, P. Strasser, *J. Electrochem. Soc.* **159**, B394 (2012)
22. M. Oezaslan, P. Strasser, *J. Power Sources* **196**, 5240 (2011)
23. F. Hasché, M. Oezaslan, P. Strasser, *Chem. Cat. Chem.* **3**, 1805 (2011)
24. K.J.J. Mayrhofer, S.J. Ashton, J.C. Meier, G.K.H. Wiberg, M. Hanzlik, M. Arenz, *J. Power Sources* **185**, 734 (2008)
25. K. Hartl, M. Hanzlik, M. Arenz, *Energy Environ. Sci.* **4**, 234 (2011)
26. K. Schlögl, M. Hanzlik, M. Arenz, *J. Electrochem. Soc.* **159**, B677 (2012)

27. K. Schlögl, K.J.J. Mayrhofer, M. Hanzlik, M. Arenz, J. Electroanal. Chem. **662**, 355 (2011)
28. F.J. Perez-Alonso, C.F. Elkjær, S.S. Shim, B.L. Abrams, I.E.L. Stephens, I. Chorkendorff, J. Power Sources **196**, 6085 (2011)
29. Y. Yu, H.L. Xin, R. Hovden, D. Wang, E.D. Rus, J.A. Mundy, D.A. Muller, H.D. Abruña, Nano. Lett. **12**, 4417 (2012)
30. J.C. Meier, I. Katsounaros, C. Galeano, H.J. Bongard, A.A. Topalov, A. Kostka, A. Karschin, F. Schüth, K.J.J. Mayrhofer, Energy Environ. Sci. **5**, 9319 (2012)
31. V. Komanicky, K.C. Chang, A. Menzel, N.M. Markovic, H. You, X. Wang, D. Myers, J. Electrochem. Soc. **153**, B446 (2006)
32. X.P. Wang, R. Kumar, D.J. Myers, Solid State Lett. **9**, A225 (2006)
33. A.O. Neto, M.J. Giz, J. Perez, E.A. Ticianelli, E.R. Gonzalez, J. Electrochem. Soc. **149**, A272 (2002)
34. F. Maillard, M. Eikerling, O.V. Cherstiouk, S. Schreier, E. Savinova, U. Stimming, Faraday Discuss. **125**, 357 (2004)
35. B. Vion-Dury, M. Chatenet, L. Guétaz, F. Maillard, ECS Trans. **41**, 697 (2011)
36. K.J.J. Mayrhofer, J.C. Meier, S.J. Ashton, G.K.H. Wiberg, F. Kraus, M. Hanzlik, M. Arenz, Electrochem. Commun. **10**, 1144 (2008)
37. L. Dubau, F. Maillard, M. Chatenet, J. André, E. Rossinot, ECS Trans. **33**, 407 (2010)
38. K. Jayasayee, J.A.R.V. Veen, T.G. Manivasagam, S. Celebi, E.J.M. Hensen, F.A. de Bruijn, Appl. Catal. B Environ. **111–112**, 515 (2012)
39. S. Mukerjee, S. Srinivasan, M.P. Soriaga, J. McBreen, J. Electrochem. Soc. **142**, 1409 (1995)
40. S. Mukerjee, J. McBreen, J. Electroanal. Chem. **448**, 163 (1998)
41. O. Antoine, Y. Bultel, R. Durand, P. Ozil, Electrochim. Acta **43**, 3681 (1998)
42. Y. Takasu, N. Ohashi, X.-G. Zhang, Y. Murakami, H. Minagawa, S. Sato, K. Yahikozawa, Electrochim. Acta **41**, 2595 (1996)